Preprints (www.preprints.org) | NOT PEER-REVIEWED | Posted: 17 March 2017 doi:10.20944/preprints201703.0141.v1

Article

The Role of Respiration in Estimation of Net Carbon Cycle: Coupling Soil Carbon Dynamics and Canopy Turnover in a Novel Version of 3D-CMCC Forest Ecosystem Model

Sergio Marconi[1,2]*, Tommaso Chiti[3,4], Angelo Nolè [5], Riccardo Valentini[2], Alessio Collalti [2,6]

1. School of Natural Resources and Environment, Institute of Food and Agricultural Sciences, University of Florida (UFL), Gainesville, US: s.marconi@ufl.edu
2. Foundation Euro-Mediterranean Center on Climate Change– Impacts on Agriculture, Forest and Ecosystem Services (IAFES), 01100 Viterbo (VT), Italy;
3. University of Tuscia – Department for Innovation in Biological, Agro-Food and Forest Systems (DIBAF), Viterbo, VT, Italy
4. Far Eastern Federal University (FEFU), Ajax St., Vladivostok, Russky Island, Russia
5. School of Agricultural, Forestry, Food and Environmental Sciences (SAFE), University of Basilicata, Italy
6. CNR-ISAFOM National Research Council of Italy, Institute for Agriculture and Forestry Systems in the Mediterranean, 87036, Rende, CS, Italy

*Correspondence: sergio.marconi@weecology.org; Tel.: +1-352-745-9685

Abstract: Understanding the dynamics of Organic Carbon mineralization is fundamental in forecasting biosphere to atmosphere Net Carbon Ecosystem Exchange (NEE). With this perspective, we developed 3D-CMCC-PSM, a new version of the hybrid Process Based Model 3D-CMCC FEM where also heterotrophic respiration (R_h) is explicitly simulated. The aim was to quantify NEE as a forward problem, by subtracting Ecosystem Respiration (R_{eco}) to Gross Primary Productivity (GPP). To do so, we developed a simplification of the Soil Carbon dynamics routine proposed in DNDC [1]. The method calculates decomposition as a function of soil moisture, temperature, state of the organic compartments, and relative abundance of microbial pools. Given the pulse dynamics of soil respiration, we introduced modifications in some of the principal constitutive relations involved in phenology and littering sub-routines. We quantified the model structure related uncertainty in NEE, by running our training simulations over 1000 random parameter-sets extracted from parameters distributions expected from literature. 3D-CMCC-PSM predictability was tested on independent time series for 6 Fluxnet sites. The model resulted in daily and monthly estimations highly consistent with the observed time series. It showed lower predictability in Mediterranean ecosystems, suggesting that it may need further improvements in addressing evapotranspiration and water dynamics.

Keywords: Forest ecosystem; Fluxnet; Soil respiration; Net ecosystem Exchange; Phenology

Preprints (www.preprints.org) | NOT PEER-REVIEWED | Posted: 17 March 2017 doi:10.20944/preprints201703.0141.v1

1. Introduction

Global concerns over increasing level of greenhouse gas concentration, particularly carbon dioxide (CO_2), pushed research efforts to better investigate biogeochemical carbon (C) fluxes dynamics and patterns between atmosphere and biosphere, and to upscale C flux estimates from site-specific to regional, continental and global scales. Increased atmospheric concentration of CO_2, combined with increasing temperatures and size variations of ecosystem C pools, are responsible for year-to-year terrestrial ecosystems carbon flux perturbations, through the variation of both photosynthetic and respiration rates [2].

In the last decades the Eddy Covariance (EC) technique provided long-term continuous measurements of Net carbon Ecosystem Exchange (NEE), water vapor and energy, within the global network of EC flux towers (FLUXNET) distributed over major terrestrial ecosystems. The availability of EC measure of NEE contributed to quantify and to determine seasonal and inter-annual variability of ecosystem C budgets at EC tower site-specific scale [3; 4; 5]. Observed NEE does not directly quantify the two major components of ecosystem C flux balance represented by ecosystem respiration (R_{eco}) and gross primary productivity (GPP). Thus, flux partitioning algorithms have been developed to partition eddy covariance NEE into photosynthetic uptake and respiratory release [6; 7]. At the same time, EC flux measurements provide key information for the parameterization, calibration and validation of process-based Forest Ecosystem Models (FEMs) contributing to large scale estimates of main ecosystem C pools.

The implementation of both forest process-based models (PBMs) [8; 9; 10; 11; 12; 13] and Functional–Structural Tree Models (FSTMs) [14; 15; 16; 17], based on the widely used Light Use Efficiency (LUE) approach [18], strongly contributed to understand and up-scale at the regional scale the analysis of the main physiological processes supporting ecosystem's C uptake. Although most of forest ecosystem models provide reliable estimates of forest growth for major terrestrial ecosystems, due to the well-established LUE approach, major limitation for NEE estimates are related to the uncertainty in R_{eco} estimation [19; 20]. In this purpose, the implementation of biogeochemical models of the C cycle based on the integration of soil respiration models and PBMs contributed to provide reliable NEE estimates [21; 22; 23]. Although soil respiration and soil organic matter (SOM) decomposition depend mainly on abiotic factors such as temperature and soil moisture [24; 25; 26], a key role is played by soil organic carbon (SOC) stock size and by the size of the microbial pools [27; 28]. In this study, we developed the 3D-CMCC-PSM (3D-CMCC-Phenology and Soil Model), a new version of the hybrid Process-Based Model 3D-CMCC FEM proposed by Collalti et al. [29; 30], where also heterotrophic respiration (R_h) is explicitly simulated to dynamically quantify stock changes of 7 different SOC pools mediated by the amount of active microbial C pools.

The aim of this study was to: i) test the performance of the modified model version, comparing model NEE estimates against independent time series for 6 Fluxnet sites, representing different forests in different climatic areas, distributed over a wide latitudinal gradient amongst European EC sites; ii) quantify uncertainty associated to the model's structure and parameterization.

2. Materials and Methods

2.1. Study Area and data

Information about forest structure and total SOC at the beginning of the simulation was collected from literature (e.g. [31; 32]) and PIs information. Sites were chosen to represent 3 diverse Forest Ecosystems, dominated by different species composition from deciduous broadleaved, DBF (i.e. *Fagus sylvatica* L.), evergreen broadleaved, EBF (i.e. *Quercus ilex* L.), and evergreen needle leaved, ENF (i.e. *Pinus sylvestris* L. and *Picea abies* L.), representing the most common European forest species from Boreal to Mediterranean Ecoregions across Europe. Eddy Covariance data were collected from FLUXNET (http://www.fluxnet.ornl.gov/fluxnet). We used EC data from different time series from daily to annual, processed using the method described in [33]. Gross Primary Production (GPP) and Ecosystem Respiration (R_{eco}) were partitioned using [6]. The sites have been chosen to represent a

Preprints (www.preprints.org) | NOT PEER-REVIEWED | Posted: 17 March 2017 doi:10.20944/preprints201703.0141.v1

climatic and longitudinal transect trough Europe, so that the model could be tested on different critical boundary conditions (Table 1).

Table 1. Sites description and stand initialization data.

Site name	Coordinates (Lat°/Lon°)	Calibration period (train set)	Simulation period (test set)	Climate	Species composition	Mean annual temperature (°C)	Mean annual precipitation (mm yr^{-1})	Mean DBH (cm)	Tree Height (m)	Stand age (years)	Stand Density (trees ha^{-1})
Puechabon (FR-Pue)	43.7/3.6	2001-03	2004-08	Mediterranean	*Quercus ilex* L. (EBF)	13.5	883	7	6	59	6149
Castelporziano (IT-Cpz)	41.7/12.3	2001-03	2004-08	Mediterranean	*Quercus ilex* L. (EBF)	15.6	780	16	12.5	45	458
Renon (IT-Ren)	46.5/11.4	2006-2008	2009-11	Temperate	*Picea abies* L. (ENF)	4.7	809	16.98	11.32	50	767
Hyytiälä (FI-Hyy)	61.8/24.2	2001-2003	2004-11	Boreal	*Pinus sylvestris* L. (ENF)	3.8	709	10.3	6.5	39	1796
Collelongo (IT-Col)	41.8/13.5	2001-2004	2005-12	Temperate	*Fagus sylvatica* L. (DBF)	6.3	1180	20.27	19.84	100	900
Hainich (DE-Hai)	51.0/10.4	2000-02	2003-07	Temperate	*Fagus sylvatica* L. (DBF)	8.3	720	30.8	23.1	120	334

2.2 Model description

The 3D-CMCC FEM is a stand-scale process-based model (PBM) designed to simulate C and water cycle in natural and managed forest ecosystems (for a full description see [29; 30]). Several eco-physiological processes are modeled within the model at species-specific level of representation and at a variable temporal scale of resolution (from daily to annual) depending on the process to simulate (Figure 1). Model outputs are generally represented at hectare scale while processes are simulated at different spatial scale from e.g. stomatal representation (e.g. stomatal conductance), canopy (e.g. canopy transpiration) and tree level (e.g. mortality) up to stand level representation (e.g. biomass stocks).

Carbon assimilation is modeled for sun and shaded leaves [1] through the land use efficiency (LUE) approach [34] constrained by environmental and stand structural (e.g. tree age) scalars [35]. Autotrophic respiration (R_A) is explicitly modeled in its components, growth and maintenance respiration (R_G and R_M, respectively). The first is computed as a fixed ratio of new growth tissues (30%) the latter is based on the nitrogen content in the biomass C pools i.e. stems, branches, leaves, fine and coarse roots, non-structural carbon (NSC), and fruits. Carbon allocation among the tree pools is controlled by species-specific parameters, phenological phase and environmental limiting factors (i.e. light and water availability). Water cycle is modeled considering the balance between ingoing (i.e. precipitation) and outgoing water (i.e. canopy transpiration and evaporation, soil evaporation and runoff). Input meteorological variables necessary to daily force the model are: global solar radiation (MJ m^{-2} day^{-1}), maximum and minimum air temperature (°C), relative humidity (%), and daily cumulated precipitation (mm day^{-1}). To be initialized model requires knowing stand structural characteristics such as: species composition, stand density, diameter at breast height (DBH), tree height and age. Soil initialization requires the estimation of Total Organic Carbon (TOC) in the different SOC pools, as described in the following section.

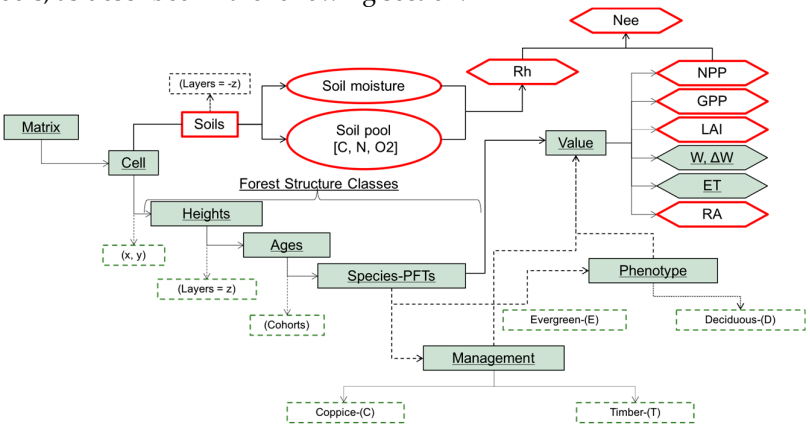

Figure 1. 3D-CMCC version PSM main flowchart modified from Collalti et al., 2014. Red circled boxes represent the pools and variable introduced or modified by 3D-CMCC-PSM.

Preprints (www.preprints.org) | NOT PEER-REVIEWED | Posted: 17 March 2017 doi:10.20944/preprints201703.0141.v1

2.2. *Model Improvements*

2.1.1. Soil Carbon Dynamics

The most recent 3D-CMC FEM model version (v.5.1, [30]) lacks in representing SOC dynamics, preventing any estimation of NEE. With that perspective, we developed a simplified version of the method described in [1] to quantify, dynamically, changes of 7 different SOC pools mediated by the amount of active microbial C pool (Figure 2).

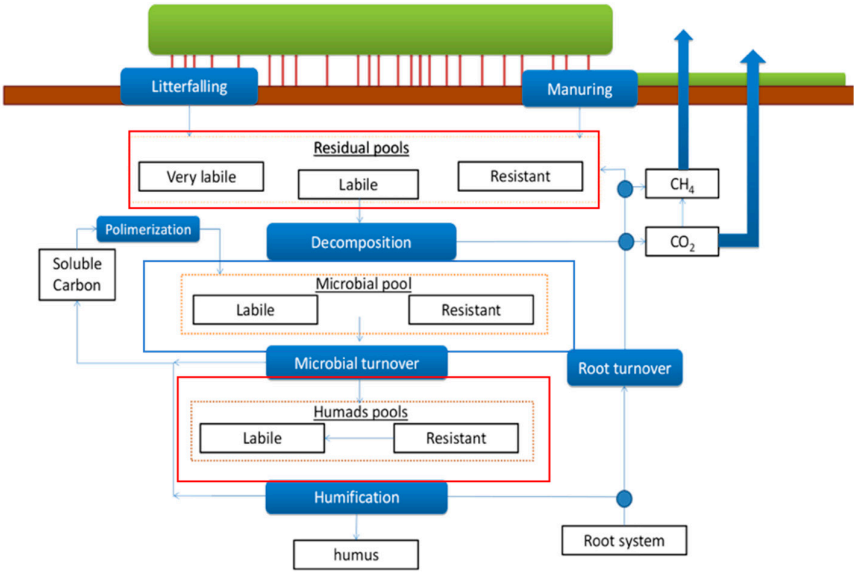

Figure 1. Soil Carbon dynamics in 3D-CMCC-PSM. The three macro pools are highlited by red boxes (dead C pool) and blue box (live C pool, i.e. microbial). Blue filled boxes represent the processes simulated by the soil model.

The litter C decomposed by microbial activity was partially mineralized as CO_2, partly stored into microbial metabolic biomass (labile), partly in structural microbial biomass (resistant) as in [1] We assumed that microbial C efficiency was constant, and specific for each C substrate pool [34]. Microbial Biomass and clay content were the principal drivers in determining the C turnover. Humic pool (we use the term Humads, to be consistent with [1]) was divided into a more labile (labile Humads, which stands for Humic acid), an intermediate (resistant Humads, which stands for Fulvic acid) and a more resistant sub-pool (Humus, which stands for Humine). Humads too were decomposed, even though at very low rates, with respect to litter and biomass pools. Inert Organic Matter (IOM) was calculated following [36].

2.1.2. Deciduous Phenology

Similarly to [30] the phenology scheme was constrained in 3 and 5 sub-phases respectively for evergreen and deciduous species (Table 2). These phases are driven by photoperiod, thermal sum, and maximum leaf biomass (resulting from maximum attainable Leaf Area Index, LAI, $m^2\ m^{-2}$).

3D-CMCC FEM represents leaves (sun and shaded) development indirectly as a by-product of alteration of class specific leaf biomass pool [37]. While the authors considered this approach a good generalization, it resulted in reducing model stability when accounting for emergent leaves respiration period in 3D-CMCC-FEM [30].

Preprints (www.preprints.org) | NOT PEER-REVIEWED | Posted: 17 March 2017 doi:10.20944/preprints201703.0141.v1

Table 2. Description of the different phenological phases for deciduous and evergreen species used in 3D-CMCC PSM.

Deciduos		Evergreen	
Phase	Trigger	Phase	Trigger
Bud Burst	GDD treshold	Bud Burst	GDD treshold
Leaf development	PeakLai/2	PeakLai	Pipe model
PeakLai	Pipe model	Leaffall	Daylength treshold
Leaffall	Daylength treshold		
Unvegetative	Delpierre et al., 2012		

We based the new Non-Structural Carbon (NSC) injection function on the hypothesis that leaves primordia demand of NSC is higher during bud burst, and gets progressively lower when maturing. Idealistically the total NSC mass (B_R) injection into early shoots, leaves and fine roots could be represented by linear differential equation (ODE):

$$\frac{\delta B_R}{\delta t} - R_{S\&F\&R}(t) \cdot B_R(t) = \quad 0, \tag{1}$$

where $R_{S\&F\&R}(t)$ is the instantaneous proportion of NSC demand for shoots and foliage growth. We assumed that C request per leaf exponentially decreases with maturity, while the total demand is positively affected by the increasing number of leaf primordia. For simplicity, we assumed that the two components resulted in a linear function. Thus:

$$\frac{R_{S\&F\&R}}{BB_T} = 1 = \quad \int_0^t \frac{B_0 \cdot t}{BB_T} \quad \delta t, \tag{2}$$

resolving the ODE by substituting $R_{S\&F\&R}(t)$ it gives:

$$\frac{\delta B_R}{\delta t} = \frac{B_0 \cdot e^{2t+2/BB_T{}^2} \cdot e^{-t^2/BB_T{}^2}}{BB_T} \quad \cdot \frac{2t}{BB_T{}^2}, \tag{3}$$

where BB_T is the parameter used in [30] for Bud Burst days (representing the number of days for a complete leaf development), $e^{2t+2/BB_T{}^2}$ is the biomass dependent and $e^{-x^2/BB_T{}^2}$ the maturity dependent factors (expressed in days). Graphically, the equation represents a skewed function of the amount of NSC allowed to be used by the trees of the specific class; the faster leaves reach maturity, the more daily specific allocation is allowed (Figure 3).

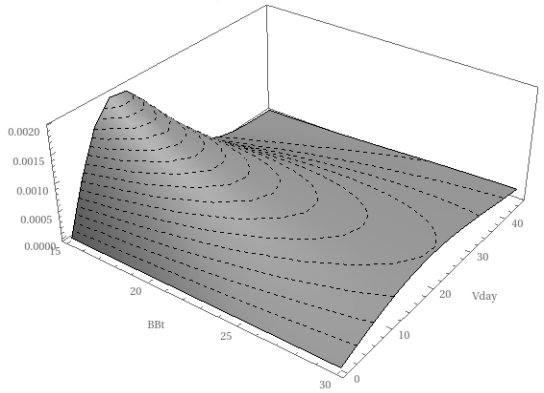

Figure 3. Graphic representation of the C injection function. The axes represent respectively bud burst days (BBt), vegetative days (Vday), and the fraction of total NSC invested in leaves development. The shorter BBt, the highet the maximum NSC fraction.

Reduction in foliage biomass during leaf-fall for deciduous forests was substituted by a new logistic function. If all leaves fall by the end of the senescence season, variation in LAI follows:

Preprints (www.preprints.org) | NOT PEER-REVIEWED | Posted: 17 March 2017 doi:10.20944/preprints201703.0141.v1

$$\frac{\partial L}{\partial t} = LAI(t) - Max\left(0, \frac{\alpha(h,a,sp)}{1+e^{\frac{t-\beta(t)}{\gamma(t)}}}\right), \quad (4)$$

$\alpha(t)$, $\beta(t)$, $\gamma(t)$ are the three parameters of the logistic function, and have a biological or physical meaning. In fact:

$$\begin{cases} \alpha(h,a,sp) = LAI_{0+\delta t}(h,a,sp) \\ \beta(s) = t_0(s) + \frac{\Delta t(s)}{2} \\ \gamma(s) \cong \frac{\Delta t(s)}{\ln(0.1) - \ln(10(\beta(s) - 0.1))} \end{cases}, \quad (5)$$

where $L_{0+\delta t}$ stands for the LAI value at peak of green, $t_0(s)$ is the first day of senescence (triggered by a species-specific day-length parameter), $\Delta t(s)$ is the length of the senescence period (days). The model calculates all these quantities using the same species-specific parameters used in the previous model version. The time derivative of the state of coloring and daily senescence, was calculated following [38] through:

$$\begin{cases} R_{sen}(t) = (T_{Max}(s) - T(t)) \cdot \left(\frac{D_L(t)}{D_L(0)}\right)^2 \\ \Delta t(s) = \sum_{R_{Sen}(t)=0}^{R_{Sen}(t)<Y_c} R_{sen}(t) \end{cases}, \quad (6)$$

where T_{Max} is a species-specific parameter representing the maximum temperature at which senescence processes is effective, $D_L(0)$ the photoperiod of the first day of senescence, $D_L(t)$ the photoperiod of the i^{th} day of the year.

2.1.3. Evergreen Phenology

Evergreen canopy turnover was modified from [30]. 3D-CMCCFEM v.5.1 assumed that evergreen leaf turnover was constant throughout the year, and that annual leaf turnover was equal to leaf biomass produced the year before [30; 37]. To better represent leaf turnover dynamics, we developed a new framework where competition for light dynamically affected leaf turnover. We hypothesized that trees optimize leaf age distribution as if they are in competition for light, in light-limited closed canopies. We used Tilman's competition for one resource conceptual model [39]:

$$\begin{cases} \frac{\partial B_i(t)}{\partial t} B_i(t)^{-1} = f_i(R) - f_i(m_i) \\ f_i(R) = \frac{r_i \cdot R}{(R + K_i)} \\ R_i^* = \frac{m_i \cdot Y_i}{(r_i - m_i)} \end{cases}, \quad (7)$$

(R_i^*) is the concentration in J m^{-2} d^{-1} of available resources (i.e. light) that a leaf requires to survive. r_i is the max photosynthetic rate (gC m^{-2} d^{-1}), m_i is the competition independent loss rate (which we considered to be Maintenance Respiration, gC m^{-2} d^{-1}), Y_i Carbon yield. The R* is the key variable to evaluate a species (or in this case a generation of leaves) average survivorship (S*), quantified as $f_i^{-1}(R_i^*)$.

We assumed for hypothesis that:

(1) Older leaves live in the shaded portions of the canopy, where light transmitted is reduced following Lambert Beer's exponential decay equation;
(2) An age dependent quasi exponential decay in leaf quantum yield efficiency;
(3) Nitrogen withdrawal from plant segments with low productivity and transfer to new leaves of higher productivity. This would cause exponential reduction in Maintenance costs for old leaves;
(4) Y_i constancy may be valid within a single tree, as the conjunctive effect of reduction in respiration rate and quantum yield efficiency.

Given these assumptions, it can be demonstrated that the survivorship rate S* of each generation of leaves ($BF_{LS(i)}$) at time *t*, is:

Preprints (www.preprints.org) | NOT PEER-REVIEWED | Posted: 17 March 2017 doi:10.20944/preprints201703.0141.v1

$$S_i^*(t) = \frac{1}{2}t^2 - \frac{2BF_{LS(i)}+1}{2}t + BF_{LS(i)}, \quad (8)$$

Leaf turnover was mainly occurring in Spring and Fall. During the bud burst season new leaves took place in the sparse crown thinned throughout Fall and Winter, aiming to crowding equilibrium. No foliar re-sprouting was simulated in Fall, even though there are evidences of it for *Quercus ilex* [40]. Leaf biomass reduction was determined by linearly decreasing each Bi to the quantity predicted by the specific parabolic decay for the end of the year.

2.1.4 Production of Fresh Organic Matter

At a relatively fine temporal scale (i.e. daily time step) the variability of litter formation, and Fresh Organic Matter (FOM) production may be fundamental in better estimating R_h [41]. We estimated FOM daily deposition as a by-product of the phenology sub-model, without increasing the number of parameters involved.

Leaves and fine root turnover were treated as processes happening in parallel, and following the same dynamics [42]. Wood turnover was not modified from [30]. Biomass coming from the aboveground deposition filled directly the Litter pool. Fresh incoming SOC was discretized in three sub-pools, representing metabolic very labile C (e.g. carbohydrates, proteins, nucleic acids and lipids), structural labile C (e.g. cellulose), and structural resistant C (e.g. lignin and complex secondary metabolites). The amount of fresh biomass entering each litter pool was estimated by the C:N ratio, as proposed by [1]:

$$\begin{cases} \frac{\partial}{\partial t}C_{i+1} = \frac{({CN_{lt}}^{-1} - {CN_i}^{-1})}{({CN_i}^{-1} - {CN_{i+1}}^{-1})} \cdot C_{lt} \\ \frac{\partial}{\partial t}C_i = \frac{\partial}{\partial t}C_{lt} - \frac{\partial}{\partial t}C_{i+1} \\ CN_i < CN_{lt} < CN_{i+1} \end{cases}, \quad (9)$$

Where C_{lt} is the C included in litter and earlier belonging to one of the 5 different structural C compartments of the plant. Its relative C and N were distributed to the two litter sub pools with proximal C:N; the former, C_{i+1}, was the one with higher recalcitrance. When CN_{lt} was higher than any litter sub pool, all the new C was added to the structural resistant pool; otherwise, if CN_{lt} was lower than the CN of the metabolic pool, all its C and N were added to the very labile sub pool. Litter C dynamically move from a pool to another. Microbes absorbed and partially immobilized litter C in their biomass, and released it again in the soil, during the humification processes [43].

2.1.5. Optimization

We introduced a new calibration scheme to provide an optimized parameterization, and quantify uncertainty related to model's structure and parameters. Calibration was performed on each site independently, using a training dataset composed by 3 years of EC daily NEE time-series (Table 1). To sample the parameterization space (i.e. the realistic values of each physiological parameter of the species simulated in each site), we randomly extracted 1,000 parameter-set combinations from prior distributions. Prior distributions were assumed to be the same among individuals of the same species, different across species. We assumed each parameter to follow a truncated normal distribution, to avoid any possibility to have negative values (i.e. non-realistic). Average and variance were estimated by using values found in literature, as in [30]. We used the same averaged value as in [30] for those parameters whose observations in literature were less than 3 (i.e. not enough to calculate sample standard deviation). The optimization was performed by choosing the parameterization set maximizing the objective function QF through:

Preprints (www.preprints.org) | NOT PEER-REVIEWED | Posted: 17 March 2017 doi:10.20944/preprints201703.0141.v1

$$QF = \left(\frac{\sum_i^n Y_i^{obs} \cdot Y_i^{sim} - \frac{\sum Y_i^{obs} \sum Y_i^{sim}}{n}}{\sqrt{\sum Y_i^{obs} - \frac{(\sum Y_i^{obs})^2}{n}} \sqrt{\sum Y_i^{sim} - \frac{(\sum Y_i^{sim})^2}{n}}} \right)^2 \times \left[1 - \frac{\sum_i^n (Y_i^{obs} - \bar{Y})^2}{\sum_i^n (Y_i^{obs} - Y_i^{sim})^2} \right] , \quad (10)$$

where Y^{Obs} represents EC daily NEE, Y^{sim} Modeled NEE for the same day. The first part of the RHS of the equation represents the square of the Pearson Correlation coefficient (R), the second the Nash-Sutcliffe Efficiency index (NSE).

2.1.6. Validation Analysis

Results were compared to Eddy Covariance data both on long-term annual average (i.e. over the full series of all the available years, ~5years), then we evaluated how the model performed in the different seasons aggregating values for months of the same season.

To evaluate the model efficiency, we calculated for daily, monthly, and seasonal: (1) R; (2) NSE; (3) Root mean square error (RMSE); and Mean Absolute Bias (MAB). Each statistic was considered differently informative [44] as summarized in Table 3. The model's ability in representing observed anomalies was determined by analyzing inter annual (IAVs) and monthly (IMVs) variability following [45] and [30].

Table 3. Statistics used for Model's results validation against Eddy Covariance data.

Statistics	Formulation	Use and ranges
Pearson Coefficient	$r = \frac{n(\sum xy) - (\sum x)(\sum y)}{\sqrt{[n\sum x^2 - (\sum x)^2][n\sum y^2 - (\sum y)^2]}}$	Estimation of model's measure of correlation with EC data [0;1]
Nash Sutcliffe efficiency	$NSE = 1 - \left[\frac{\sum_{i=1}^n (Y_i^{obs} - Y_i^{sim})^2}{\sum_{i=1}^n (Y_i^{obs} - \bar{Y})^2} \right]$	Estimation of model's predictability [-∞;1]
Root Mean Square Error	$RMSE = \sqrt{\frac{\sum_{\tau=1}^n (y_\tau - y_\tau)^2}{n}}$	Estimation of model's accuracy gC m^{-2} d^{-1} [0; ∞]
Mean Absolute Bias	$MAB = \sum_{i=1}^N \left(\frac{\lvert Y_{MD_i} - Y_{EC_i} \rvert}{\sigma(Y_{EC_i})} \right) \frac{1}{N}$	Estimation of model's bias gC m^{-2} d^{-1} [0; ∞]

3. Results

3.1. Evaluation of daily, seasonal, and annual NEE estimations

To evaluate 3D-CMCC-PEM NEE predictions, we compared predicted (MD) daily and monthly NEE time series to EC daily data. The analyses were performed only on the test data (i.e. portions of the series which have not been used for calibration) to avoid any effect of overfitting. The model showed high correlations with observed EC data at all sites for both daily and monthly fluxes, apart from ITCpz site (Table 4). Excluding ITCpz, R ranged at all sites from 0.65 to 0.84 for daily and, 0.59 to 0.97 for monthly scale. Beech dominated Deciduous Forests (DBF) performed better than Conifer species (ENF) and evergreen Mediterranean broadleaved forests (EBF). ENF and EBF in FRPue performed similarly on daily scale, for all the statistics used. However, ENF predictability significantly increased on monthly scale (R ranging between 0.92 and 0.97), while EBF performed worse (R 0.42 in ITCpz, and 0.59 in FRPue). RMSE on average was 1.92 gC m^{-2} d^{-1}. MAE ranged between 0.96 and 1.78 gC m^{-2} d^{-1}, and on average it decreased almost twice on monthly timescale. MAB showed similar behavior for DBF and ENF. It ranged between 0.39 and 0.56 gC m^{-2} d^{-1} (0.50 on average) for daily time series. Mediterranean forests resulted the ones with highest MAB, and showed no significant reduction when predictions were aggregated on monthly scale. Differently from the other simulations, even NSE just improved slightly for ITCpz, and even reduced for FRPue simulation.

Preprints (www.preprints.org) | NOT PEER-REVIEWED | Posted: 17 March 2017 doi:10.20944/preprints201703.0141.v1

Table 4. Daily and Monthly Validation statistics calculated on the test-set. As stated in Table 3, R and NSE are dimensional; RMSE and MAB are gC m^{-2} d^{-1}.

	DEHai	ITCol	FIHyy	ITRen	ITCpz	FRPue	Mean
Daily NEE							
R	0.84	0.76	0.67	0.65	0.24	0.65	0.64
NSE	0.67	0.5	0.34	0.21	-0.26	0.35	0.3
RMSE	1.84	2.7	1.48	2.32	1.8	1.39	1.92
MAB	0.39	0.5	0.53	0.56	1.15	0.76	0.65
Monthly NEE							
R	0.93	0.92	0.96	0.97	0.42	0.59	0.8
NSE	0.81	0.76	0.9	0.87	0.12	0.2	0.61
RMSE	1.15	1.58	0.45	0.72	1.24	1	1.02
MAB	0.28	0.32	0.21	0.24	1.25	0.86	0.53

Daily results were aggregated in seasonal series to evaluate seasonal predictability. Seasonal aggregations showed that 3D-CMCC-PEM poorly performs in predicting seasonal fluxes. NSF was generally negative in Summer, with the exclusion of DEHai and FRPue. 3D-CMCC-PEM generally best reproduced NEE dynamics in Fall (R ranging between 0.22 and 0.89). ENF ecosystems showed consistently higher correlation in Spring predictions, with R of 0.65 and MAB of 0.62 gC m^{-2} d^{-1} on average. In the case of evergreen stands, 3D-CMCC-PEM consistently showed poor performance in Summer. Expectedly, DBF performed the worst in Winter (Table 4). NSE on average resulted positive only in Fall for both DBF and EBF, and Spring, for ENF stands.

Table 5. Seasonal validation statistics calculated on the test-sets and aggregated by ecosystem type. As stated in Table 3 and 4, R and NSE are dimensional; RMSE and MAB are gC m^{-2} d^{-1}.

	R	NSE	RMSE	MAB
DBF				
MAM	0.43	-0.36	2.77	0.72
JJA	0.36	-0.02	2.96	1.17
SON	0.82	0.58	1.9	0.58
DJF	0.2	-0.93	0.7	1.58
EBF				
MAM	0.65	0.28	1.83	0.62
JJA	0.11	-0.92	2.76	1.01
SON	0.51	0.03	1.56	0.74
DJF	0.38	-1.59	0.51	0.82
ENF				
MAM	0.18	-0.41	1.95	1.2
JJA	0.32	-0.34	1.58	1
SON	0.45	-0.19	1.3	0.79
DJF	0.47	-6.13	1.45	1.4

Taylor diagrams [46] showed that 3D-CMCC-PEM performance was generally satisfactory (Figure 4). Daily simulations resulted in all sites but ITCpz being within the ±1 normalized standard deviation region. Monthly scale predictions were more consistent with EC data, especially for BDF and ENF sites. It resulted in all 4 simulations falling within ±0.5 normalized standard deviation from the reference point, and R > 0.9 (Figure 2). Again, 3D-CMCC-PEM performed worst in EBF, with FRPue still inside ±1 normalized standard deviation region, and ITCpz falling outside the ±1.5 normalized SD region. The consistently worse predictability in ITCpz and FRPue confirm a systematic weakness in 3D-CMCC to represent fluxes for these sites as already described in [30]. Model performance on annual scale showed a different pattern, mostly because of some sites

Preprints (www.preprints.org) | NOT PEER-REVIEWED | Posted: 17 March 2017 doi:10.20944/preprints201703.0141.v1

consistent biases in seasonal NEE, and the difference in NEE magnitude. Delay in Spring phenology, and the consistent underestimation of Summer NEE, resulted in significant underestimation and scarce predictability of ITCol annual NEE ($R < 0.2$). ITCPz and FRPue resulted among the sites with higher annual predictability, partly because of the low seasonal variance in NEE, partly because Winter and Spring bias tends to compensate each other.

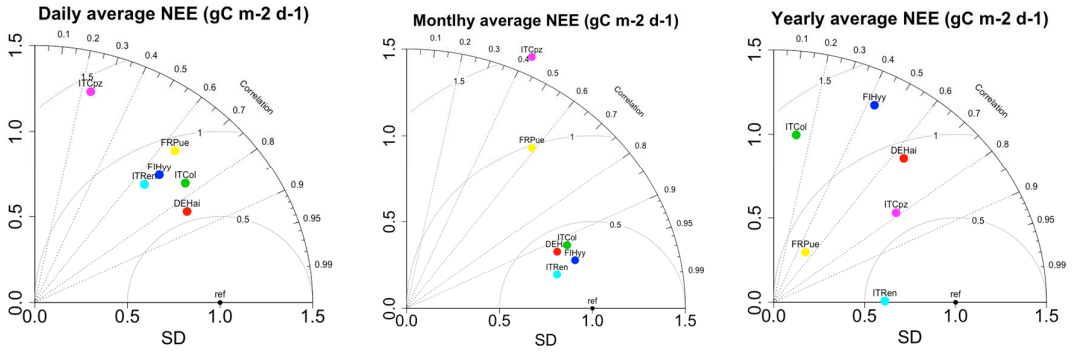

Figure 4. Taylor diagram representing 3D-CMCC-PSM performance in (a) daily, (b) monthly and (c) annual NEE estimation for the test-set.

3.2. Anomalies and parameters related uncertainty

Figure 5 shows uncertainty associated to random choice of parameters. Overall, uncertainty was expectedly higher in Summer and Fall. Such increase was particularly clear for deciduous forests, which not only showed wider NEE standard deviation, but also had optimal modeled NEE falling outside standard deviation area.

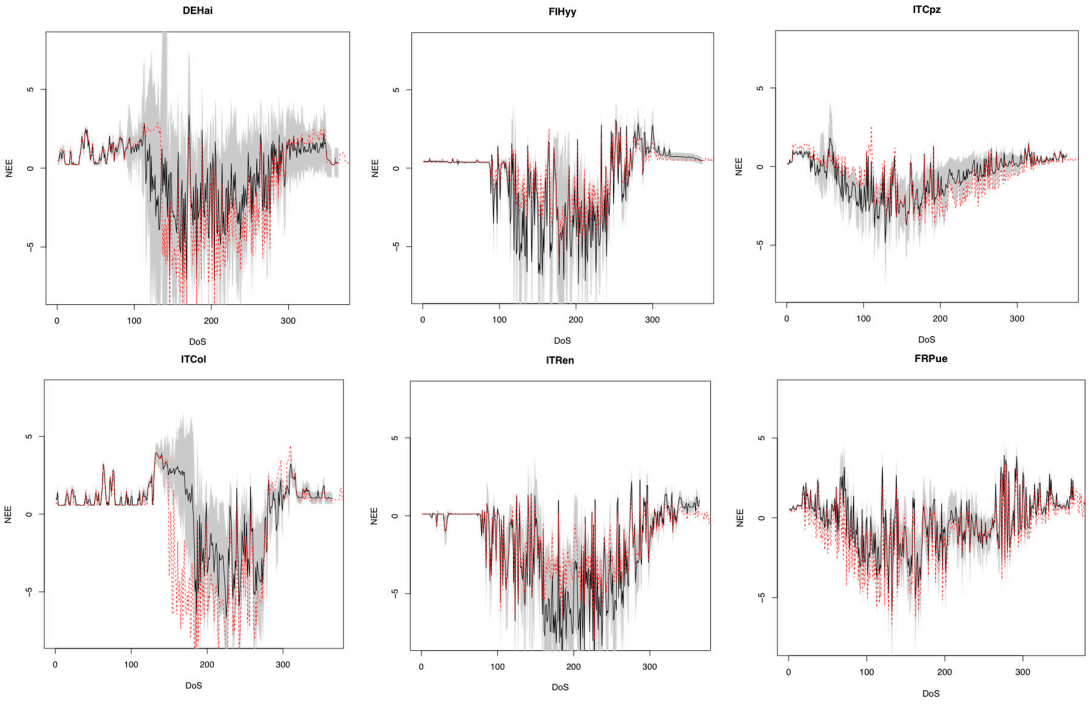

Figure 5. Model structure related uncertainty in estimating NEE (gC m^{-2} d^{-1}) per DoY (Day of Year) by a random choice of parameters values from prior distributions. Data represent 300 1-year simulations from randomly extracted parameterization-sets. Average daily simulations (black line) and standard deviation (grey area). Red dotted line represents daily NEE simulation for the optimized parameterization set.

Preprints (www.preprints.org) | NOT PEER-REVIEWED | Posted: 17 March 2017 doi:10.20944/preprints201703.0141.v1

DBF sites showed also high uncertainty in estimating the first vegetative day, suggesting that a better representation of Winter dormancy effects on bud burst dates may significantly improve model's predictability. Uncertainty was generally lower in Mediterranean sites, despite model's performance was generally lower. 3D-CMCC-PSM uncertainty was generally low for ENF for most of the year, but was generally high when Temperature were higher. Higher uncertainty for warmer days was generally found in DBF sites too, suggesting that 3D-CMCC-PSM was expectedly sensitive to high Temperatures for both Photosynthesis [47] and Respiration [48], but these effects didn't always compensate each other.

NEE inter-annual variability was generally underestimated by the model. Nevertheless, 3D-CMCC-PSM correctly reproduced 81% of the sign of the anomalies, and residuals difference in magnitude was usually less than 0.3 gC m^{-2} d^{-1}. Highest difference in magnitude occurred in ITCol (difference in residuals higher than 0.5 gC m^{-2} d^{-1} in 5 years out of 12). Highest difference was shown in ITCpz, where the sign was correctly reproduced only once out of 8 years, and having more than 1gC m^{-2} d^{-1} of residual difference. Inter-monthly variability (IMV) showed species-specific patterns. DBF had higher IMV mismatches in May and late Summer (i.e. August in DEHai, July in ITCol). Despite the average IMV was well represented for ENF, the model showed less IMV predictability mainly in Winter (e.g. November and January) and Summer (e.g. August). EBF showed the worst predictability of IMV average and variance, despite the reduced seasonality compared to the other sites (Figure 6).

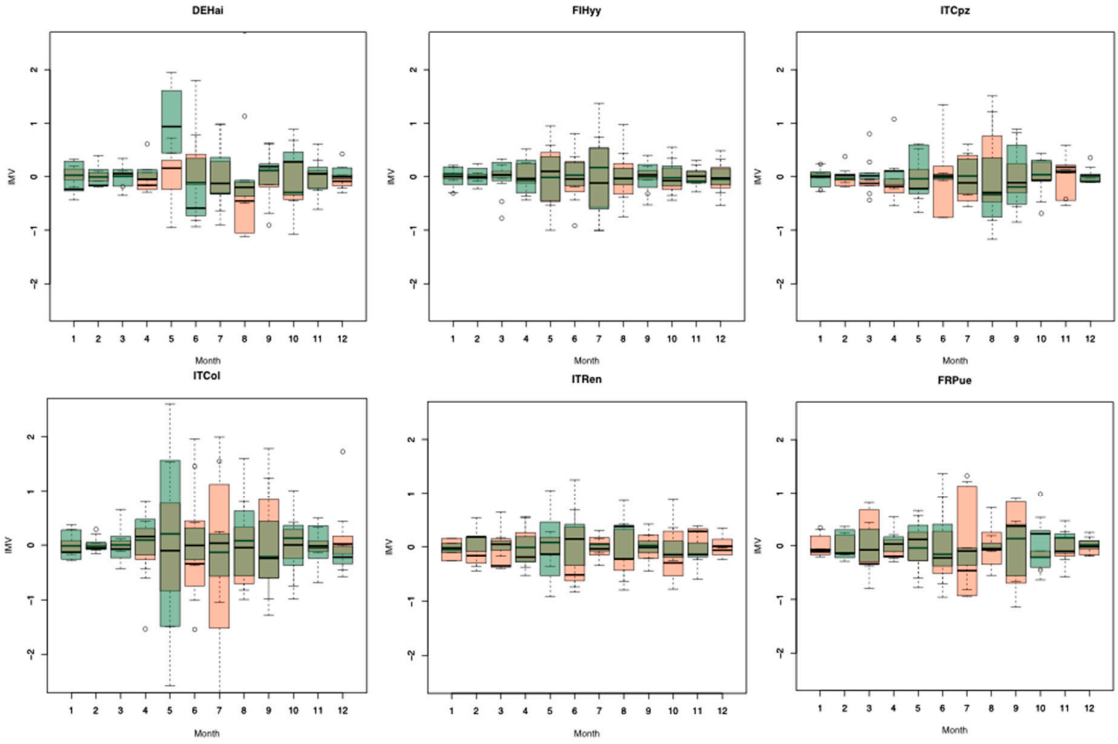

Figure 6. Inter monthly variability (MV) for the test time-series (gC m^{-2} $month^{-1}$). Observed IMV in green boxes, simulated IMV in orange.

4. Discussion

The ideas brought by 3D-CMCC-PSM overall produced significant improvements in representing the net C cycle of the studied forest ecosystems. The aim of this study was not testing how better the model performed in estimating gross primary production (GPP), hence we didn't provide a deep

Preprints (www.preprints.org) | NOT PEER-REVIEWED | Posted: 17 March 2017 doi:10.20944/preprints201703.0141.v1

comparison with the last version (i.e. 3D-CMCC-FEM v.5.1). However, we observed that 3D-CMCC-PSM resulted in better estimation of GPP, especially for ENF IAVs and IMVs (data not showed).

4.1. 3D-CMCC-PSM predictability in estimating NEE

In general, the inclusion of a simplistic SOC routine resulted in a reliable estimation of daily and monthly NEE trends. While daily and monthly trends are consistent with EC data, seasonal patterns showed non-negligible misrepresentations, which resulted in negative NSE in most of the cases. This inconsistency may be driven by the strong seasonality in both R_{eco} and GPP [49], which positively affects correlation between EC data and MD results.

NEE trends during Summer and Fall were much more consistent with the measured ones, than Winter and Spring trends. During these seasons the biases appeared mostly affected by estimation of R_{eco}. The scarcity of the model in representing EBF C fluxes was especially attributable to GPP predictions. 3D-CMCC-PSM and 3D-CMCC FEM inability in predicting GPP in ITCpz and FRPue sites, denoted the necessity to better represent the relations between Mediterranean forests and environmental factors [50; 51]. In FRPue the model well reproduced Spring, Summer and Fall NEE. On the other hand, it showed a bias of around 1gC m-2 d-1 in Winter, suggesting it was missing some particularly important seasonal processes. For example, evergreen phenology still didn't consider secondary or continuous growth. Thus, species like Quercus ilex, which exhibit secondary gem sprout in Fall [40], have fresh leaves and mild temperatures to guarantee photosynthetic activity in Fall and Winter, partly explaining 3D-CMCC FEM and 3D-CMCC-PSM systematic underestimation.

ITCpz showed the same pattern. However, differently from FRPue, it poorly performed also in early Spring and Summer, especially for GPP patterns. This misbehavior was expected, because of the physical characteristics of the site. In fact, 3D-CMCC FEM soil water dynamics routine was still simplistic, and to date, such other similar models, didn't include any effect of water table dynamics. On the contrary, ITCpz is characterized with the presence of a shallow groundwater table, which seems to reduce water stress in early Summer [30].

Summer IMVs misrepresentation in DBF was probably affected by the assumption that LAI and photosynthetic capacity reach their maximum in early Summer, alongside. On the contrary, maximum photosynthetic capacity may be reached in late summer, and vary across the canopy. Without taking this into account, GPP could be overestimated up to 40% [52]. Notwithstanding, comparing model outputs with published works [53; 54] these defects are common also for other PBMs.

Seasonal patterns showed that the model consistently misrepresented NEE in Winter, suggesting that R_{eco} still needs to be improved. Especially for DBF sites (e.g. DEHai), Winter R_{eco} is mostly driven by RH. RH is exponentially affected by soil temperatures and especially moisture [55], which are calculated by the model, and could be over-fluctuating in Winter. Moreover, EC data are prone to random noise [56], whose relative impact on performance metrics may be relatively larger.

Interestingly, annual predictions suggested reasonably high performance of 3D-CMCC-PSM, despite these seasonal inconsistencies. This suggests that biases are usually consistent within a season, but have different sign across seasons (Figure 7), resulting in a compensating effect at coarser time scale.

Preprints (www.preprints.org) | NOT PEER-REVIEWED | Posted: 17 March 2017 doi:10.20944/preprints201703.0141.v1

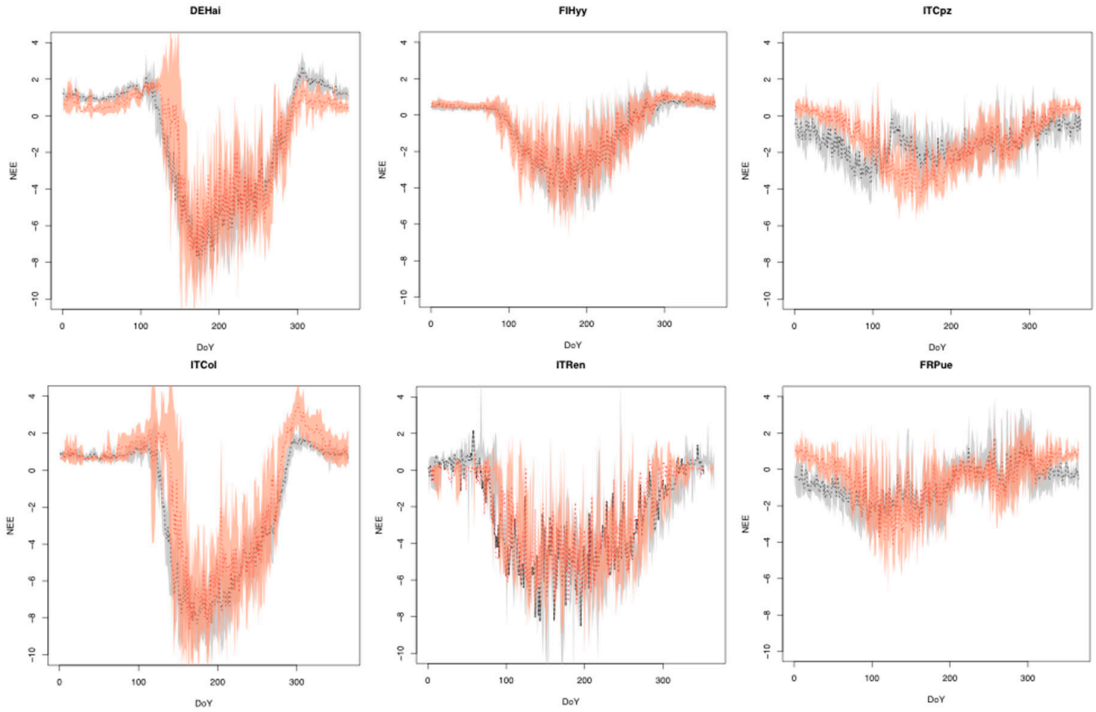

Figure 7. Trends in daily NEE (units) per DoY (Day of Year) calculated from test-sets on a site level. Observed EC average trends (black dotted line) and standard deviation (gray area). Simulated average trends (red dotted line) and standard deviation (orange area).

It was not always possible to individually validate the different components of respiration. However, the results of R_{eco} comparison with EC data, the NPP:GPP consistency with literature [57; 58; 59], showed that the new 3D-CMCC-FEM version was able to reproduce respiration processes well enough, especially on monthly timescale.

Soil respiration seems to be overestimated during Summer, implying a systematic overestimation of NEE. This was especially true in ITCol. Since no significant pulse in FOM happened in that period, this misbehavior may be related to the use of the exponential relationship between respiration, moisture, and temperature [47].

Lack of data to validate the SOC dynamics reduced the spectrum of speculations, which could be statistically analyzed. SOC didn't change its quantity in ten years; this result was consistent with the theoretical stability of the SOC, an indicator which rarely change within 10 years if no strong disturbance event (e.g. land use change) have occurred [60]. Litter C was highly fluctuating within a year, but its quantity was stable if compared at the end of each year. This suggested that the model realistically represented litter turnover and decomposition, since residues were degraded into humus labile substances about within a year [61]. Microbial Biomass was highly variable, as expected. However, the magnitude of change was too broad throughout the simulations. These results may be related to the use of 5% as the initial active microbial biomass for each site, value that may be far from the equilibrium for different soils. Moreover, tradeoffs within microbial growth and between the environmental conditions may be scarcely represented. As a matter of fact, 3D-CMCC-PSM simulated the soil as having the same physical-chemical structure throughout the profile. This implied that microbes could find the same amount of C, O2, and living space, with no depth limitation.

4.2. 3D-CMCC-PSM uncertainty in estimating NEE

Preprints (www.preprints.org) | NOT PEER-REVIEWED | Posted: 17 March 2017 doi:10.20944/preprints201703.0141.v1

We analyzed 300 random parameterization-sets per site to quantify model assumptions and uncertainty. The model showed different behavior in different sites, but expectedly consistent across species behaving in a similar functional way. These results may suggest that using functional traits combinations to provide physiological parameters, instead of fixed species-specific ones, may produce still reliable and more general predictions, particularly useful in case of larger spatial/ temporal simulations [62; 63; 64]. Using a species-level parameterization, in fact, may result in a too fine "resolution" because: (1) it would require excessive computational resources and a finely detailed parameterization, usually inaccessible on broad scale [65]; (2) the model's rationale in predicting forest structure is mainly driven by competition for resources. However, there are not explicit tradeoffs, positive interactions between different tree cohorts, or intra-specific traits variability, which are fundamental to forecast forest ecosystem structure on long-run simulations [66]. Having fixed species-specific parameters throughout century would potentially result that only a very reduced amount of species would dominate the different cohorts on landscape to regional scale

According to Figures 5 and 6, strong uncertainties still reside in timing for the different phenological phases. The biggest source of uncertainty in deciduous stands was driven by the amount of degree days needed to begin vegetative period. The use of a site-specific thermal sun (GDD) to activate vegetation period is widely used, but proven to be very site sensitive, and not very effective for a regional generalization [67]. On the other hand, the processes triggering bud-burst timing are still partly unknown. Moreover, those models proposing a process oriented promoter-inhibition rationale are generally over complex and not prone to spatial generalization [68]. A possible solution in this context is to use remotely sensed data to train a latitudinal explicit regression, constraining GDD estimation.

3D-CMCC-PSM showed high uncertainty also in catching the beginning of the senescence phase. The new phenological scheme didn't reduce such uncertainty, since it was still using a photoperiod threshold as the senescence phase trigger [30]. Another strong source of uncertainty in Summer GPP may be held by the over simplicity of soil structure and thus of the soil water routine.

As shown in [30], EC data are prone to high uncertainty. We focused on NEE fluxes to reduce the uncertainty cascade related to NEE partitioning. The next natural step will be reframing the model with a hierarchical Bayesian fashion, to quantify error propagation and parameters uncertainty from the posterior distribution [69].

Daily R_{eco} estimation was affected by the cascade of uncertainties related to the calculation of R_A and heterotrophic, calculated independently. R_A routine may strongly be influenced by uncertainties in R_M estimation, which often resulted in R_A overestimation. The R_M was in fact simulated by a set of empirical relations, which involve: (1) the use of a fixed non-acclimating Q10 factor, whose generality is known to be inaccurate [70]. Moreover, the rationale of Ryan's R_M calculation [71] is affected by uncertainty in estimating daily increment of N pools, generally estimated by forest ecosystem models as a fixed proportion of daily C increment.

5. Conclusions

Soil respiration has a key role in determining NEE in a deterministic In general, this works showed how the inclusion of a simplistic Soil Carbon routine improved the allowed to predict trends and variability of NEE across the most diffuse European forest ecosystems. The modifications in the phenology scheme resulted in improvements in 3D-CMCC FEM uncertainty in Fall and Spring, but were still limited by the correct estimation of each phenological phase (e.g. bud burst timing, leaf senescence starting point and length). The use of an optimized parameter-set improved the model's performance only for those sites where the bio-geophysical processes were correctly reproduced. As a matter of fact, we showed how Mediterranean terrestrial forests, which showed lacks in representing some biological and/or physical processes, performed significantly worse than the other sites, regardless the use of optimized parameters.

Preprints (www.preprints.org) | NOT PEER-REVIEWED | Posted: 17 March 2017 doi:10.20944/preprints201703.0141.v1

In conclusion, we think that 3D-CMCC-PSM reliably estimated NEE and R_{eco} dynamic in a forest ecosystem, especially scaling up daily results to monthly NEE averages. We think that 3D-CMCC-PSM is a solid basis to further explore the effects of soil structure on Carbon and Water dynamics, especially in Mediterranean systems, and be used as a tool for predicting forest growth and ecosystem services, and address questions related to future scenarios forecasting.

Acknowledgements

S.M. was partially supported by the Gordon and Betty Moore Foundation's Data-Driven Discovery Initiative through Grant GBMF4563 to Ethan P. White, and by the GEMINA project to CMCC.

A.C. was partially supported by the European Union's Horizon 2020 research and innovation program under grant agreement N. 641816 (CRESCENDO project; http://crescendoproject.eu/) and by the "ALForLab" (PON03PE_00024_1) project co-funded by the National Operational Program for Research and Competitiveness (PON R&C) 2007-2013, through the European Regional Development Fund (ERDF) and national resource (Revolving Fund - Cohesion Action Plan (CAP) MIUR.

This work used eddy covariance data acquired and shared by the FLUXNET community, including these networks: AmeriFlux, AfriFlux, AsiaFlux, CarboAfrica, CarboEuropeIP, CarboItaly, CarboMont, ChinaFlux, Fluxnet-Canada, GreenGrass, ICOS, KoFlux, LBA, NECC, OzFlux-TERN, TCOS-Siberia, and USCCC. The ERA-Interim reanalysis data are provided by ECMWF and processed by LSCE. The FLUXNET eddy covariance data processing and harmonization was carried out by the European Fluxes Database Cluster, AmeriFlux Management Project, and Fluxdata project of FLUXNET, with the support of CDIAC and ICOS Ecosystem Thematic Center, and the OzFlux, ChinaFlux and AsiaFlux offices.

We acknowledge Ethan P. White and Monia Santini for providing critical comments. Carlo Trotta and Giorgio Matteucci for insights about the use of Eddy Covariance data.

Author Contributions: S.M. conceived the project, designed the experiments, co-developed the model code, performed the simulations, analyzed the data, and wrote the manuscript. A.C. contributed in designing the experiment, co-developed the model code, and writing the manuscript. T.C. contributed in writing the manuscript. A.N. contributed in writing the manuscript. R.V. contributed in writing the manuscript.

Conflicts of Interest:

The authors declare no conflict of interest.

References

1. Zhang, Y., Li, C., Zhou, X., & Moore, B. (2002). A simulation model linking crop growth and soil biogeochemistry for sustainable agriculture. Ecological Modelling, 151(1), 75-108.
2. Baldocchi D, Ryu Y and Keenan T. Terrestrial Carbon Cycle Variability [version 1; referees: 2 approved]. F1000Research 2016, 5(F1000 Faculty Rev):2371 (doi: 10.12688/f1000research.8962.1)
3. Göckede M, Foken T, Aubinet M, Aurela M, Banza J, Bernhofer C, et al. 2008, Quality control of CarboEurope flux data – Part 1: Coupling footprint analyses with flux data quality assessment to evaluate sites in forest ecosystems. Biogeosciences, 5(2):433–50. doi: 10.5194/bg-5-433-2008.
4. Xiao J, Zhuang Q, Law BE, Chen J, Baldocchi DD, Cook DR et al. (2010) A continuous measure of gross primary production for the conterminous U.S. derived from MODIS and AmeriFlux data. Remote Sens Environ 114:576–591 http://dx.doi.org/10.1016/j.rse.2009.10.013.
5. Tang XG, Liu DW, Song KS, Munger JW, Zhang B, Wang ZM (2011) A new model of net ecosystem carbon exchange for the deciduous-dominated forest by integrating MODIS and flux data. Ecol Eng 37:1567–1571
6. Reichstein, M., Falge, E., Baldocchi, D.D., Papale, D., Valentini, R., Aubinet, M., Berbigier, P., Bernhofer, C., Buchmann, N., Gilmanov, T., Granier, A., Gru¨nwald, T., Havra´nkova´, K., Ilvesniemi, H., Janous, D., Knohl, A., Laurela, T., Lohila, A., Loustau, D., Matteucci, G., Meyers, T., Miglietta, F., Ourcival, J.-M., Pumpanen, J., Rambal, S., Rotenberg, E., Sanz, M., Tenhunen, J., Seufert, G., Vaccari, F., Vesala, T., Yakir, D., and Valentini, R. 2005. On the separation of net ecosystem exchange into assimilation and ecosystem respiration: review and improved algorithm. Glob. Change Biol. 11(9): 1–16. doi:10.1111/j.1365-2486. 2005.001002.x.
7. Lasslop, G., Migliavacca, M., Bohrer, G., Reichstein, M., Bahn, M., Ibrom, A., Jacobs, C., Kolari, P., Papale, D., Vesala, T., Wohlfahrt, G., and Cescatti, A. 2012. On the choice of the driving temperature for eddy-covariance carbon dioxide flux partitioning, Biogeosciences, 9, 5243-5259, doi:10.5194/bg-9-5243-2012,

Preprints (www.preprints.org) | NOT PEER-REVIEWED | Posted: 17 March 2017 doi:10.20944/preprints201703.0141.v1

8. Potter, C.S., Randerson, J.T., Field, C.B., Matson, P.A., Vitousek, P.M., Mooney, H.A., Klooster, S.A., 1993. Terrestrial ecosystem production: a process model based on global satellite and surface data. Global Biogeochem. Cycles 74, 811–841
9. Prince, S.D., Goward, S.N., 1995. Global primary production: a remote sensing approach. J. Biogeogr. 22, 815–835.
10. Mäkelä, A., Landsberg, J., Ek, A.R., Burk, T.E., Ter-Mikaelian, M., et al., 2000. Process-based models for forest ecosystem management: current state of the art and challenges for practical implementation. Tree Physiology 20, 289–298.
11. Yuan, W.P., Liu, S.G., Zhou, G.S., Zhou, G.Y., Tieszen, L.L., Baldocchi, D., Bernhofer, C., Gholz, H., Goldstein, A.H., Goulden, M.L., Hollinger, D.Y., Hu, Y., Lawn, B.E., Stoy, P.C., Vesala, T., Wofsy, S.C., 2007. Deriving a light use efficiency model from eddy covariance flux data for predicting daily gross primary production across biomes. Agric. Forest Meteorol. 1433, 189–207.
12. Yuan, W, Cai, W, Xia, J, Chen, J, Liu, S, Dong, W, Merbold, L, Law, B, Arain, A, Beringer, J, Bernhofer, C, Black, A, Blanken, PD, Cescatti, A, Chen, Y, Francois, L, Gianelle, D, Janssens, IA, Jung, M, Kato, T, Kiely, G, Liu, D, Marcolla, B, Montagnani, L, Raschi, A, Roupsard, O, Varlagin, A & Wohlfahrt, G. 2014. Global comparison of light use efficiency models for simulating terrestrial vegetation gross primary production based on the LaThuile database' Agricultural and Forest Meteorology, vol 192-193, pp. 108-120. DOI: 10.1016/j.agrformet.2014.03.007
13. Cai, W.W., Yuan, W.P., Liang, S.L., Zhang, X.T., Dong, W.J., Xia, J.Z., Fu, Y., Chen, Y., Liu, D., Zhang, Q., 2014. Improved estimations of gross primary production using satellite-derived photosynthetically active radiation. J. Geophys. Res.: Biosci. 119, http://dx.doi.org/10.1002/2013JG002456.
14. Lacointe, A., 2000. Carbon allocation among tree organs. A review of basic processesand representation in functional-structural tree models. Annals of Forest Science57, 521–533.
15. Sievänen R., Nikinmaa E., Nygren P., Ozier-Lafontaine H., Perttunen J., et al. (2000). Components of functional-structural tree models. Annals of Forest Science, Springer Verlag, 57 (5), pp.399-412
16. Lu, M., Nygren, P., Perttunen, J., Pallardy, S.G. & Larsen, D.R. (2011). Application of the functional-structural tree model LIGNUM to growth simulation of short-rotation eastern cottonwood. Silva Fennica 45(3): 431–474
17. Nikinmaa E, Sievänen R, Hölttä T. Dynamics of leaf gas exchange, xylem and phloem transport, water potential and carbohydrate concentration in a realistic 3-D model tree crown. Annals of Botany. 2014;114 653–666.
18. Monteith, J. and Moss, C. J. (1977) Climate and the efficiency of crop production in Britain, Philos. T.R. Soc. Lond., 281, 277–294, doi:10.1098/rstb.1977.0140.
19. Trumbore S. 2006. Carbon respired by terrestrial ecosystems-recent progress and challenges. Global Change Biol., 12 (2006), pp. 141–153
20. Mitchell, S., Beven, K., Freer, J. 2009. Multiple sources of predictive uncertainty in modeled estimates of net ecosystem CO2 exchange, Ecological Modelling, 220, 3259-3270, ISSN 0304-3800, http://dx.doi.org/10.1016/j.ecolmodel.2009.08.021.
21. Yuan, F., Arain, M.A., Barr, A.G., Black, T.A., Bourque, C.P.A., Coursolle, C., Margolis, H.A., Mccaughey, J.H. and Wofsy, S.C. (2008), Modeling analysis of primary controls on net ecosystem productivity of seven boreal and temperate coniferous forests across a continental transect. Global Change Biology, 14: 1765–1784. doi:10.1111/j.1365-2486.2008.01612.x
22. Xu, B., Y. Yang, P. Li, H. Shen, and J. Fang (2014), Global patterns of ecosystem carbon flux in forests: A biometric databased synthesis, Global Biogeochem. Cycles, 28, 962–973, doi:10.1002/ 2013GB004593.
23. Zobitz, J. M., Moore, D. J. P., Sacks, W. J., Monson, R. K., Bowling, D. R., & Schimel, D. S. (2008). Integration of process-based soil respiration models with whole-ecosystem CO2 measurements. Ecosystems, 11(2), 250-269. DOI: 10.1007/s10021-007-9120-1
24. Lloyd, J., and Taylor, J.A. 1994. On the temperature dependence of soil respiration. Funct. Ecol. 8(3): 315–323. doi:10.2307/2389824.
25. Kirschbaum, M.U.F. 2004. Soil respiration under prolonged soil warming: are rate reductions caused by acclimation or substrate loss? Global Change Biology, 10, pp. 1870–1877
26. Xu, J., Chen, J., Brosofske, K., Li, Q., Weintraub, M., Henderson, R., Wilske, B., John, R., Jensen, R., Li, H. et al. 2011. Influence of timber harvesting alternatives on forest soil respiration and its biophysical regulatory factors over a 5-year period in the Missouri Ozarks, Ecosystems, 14, 1310–1327,.
27. Schimel, J. P., and M. N. Weintraub (2003), Soil organic matter does not break itself down the implications of exoenzyme activity on microbial carbon and nitrogen limitation in soil: A theoretical model, Soil Biol. Biochem., 35, 549–563.

Preprints (www.preprints.org) | NOT PEER-REVIEWED | Posted: 17 March 2017 doi:10.20944/preprints201703.0141.v1

28. Tian, H., C. Lu, J. Yang, K. Banger, D. N. Huntzinger, C. R. Schwalm, A. M. Michalak, R. Cook, P. Ciais, D. Hayes, et al. (2015), Global patterns and controls of soil organic carbon dynamics as simulated by multiple terrestrial biosphere models: Current status and future directions, Global Biogeochem. Cycles, 29, 775–792. doi:10.1002/2014GB005021.
29. Collalti, A., Perugini, L., Santini, M., Chiti, T., Nolè, A., Matteucci, G., & Valentini, R. (2014). A process-based model to simulate growth in forests with complex structure: Evaluation and use of 3D-CMCC Forest Ecosystem Model in a deciduous forest in Central Italy. Ecological Modelling, 272, 362-378.
30. Collalti, A., Marconi, S., Ibrom, A., Trotta, C., Anav, A., D'andrea, E., ... & Grünwald, T. (2016). Validation of 3D-CMCC Forest Ecosystem Model (v. 5.1) against eddy covariance data for 10 European forest sites. Geoscientific Model Development, 9(2), 479-504.
31. Mencuccini, M., & Bonosi, L. (2001). Leaf/sapwood area ratios in Scots pine show acclimation across Europe. Canadian Journal of Forest Research, 31(3), 442-456.
32. Pilegaard, Kim, Teis N Mikkelsen, Claus Beier, Niels Otto Jensen, Per Ambus, and Helge Ro-poulsen. (2003). "Field Measurements of Atmosphere– Biosphere Interactions in a Danish Beech Forest", no. December: 315–33.
33. Papale, D., Reichstein, M., Aubinet, M., Canfora, E., Bernhofer, C., Longdoz, B., Kutsch, W., Rambal, S., Valentini, R., Vesala, T., Yakir, D., 2006. Towards a standardized processing of Net Ecosystem Exchange measured with eddy covariance technique: algorithms and uncertainty estimation. Biogeosciences 3, 571–583.
34. Landsberg J.J., Waring R.H. (1997). A generalised model of forest productivity using simplified concepts of radiation-use efficiency, carbon balance and partitioning. Forest Ecology and Management. vol. 95, p. 209-228.
35. Molina, J. A. E., C. E. Clapp, M. J. Shaffer, F. W. Chichester, and W. E. Larson. (1983). "NCSOIL, A Model of Nitrogen and Carbon Transformations in Soil: Description, Calibration, and Behavior1." Soil Science Society of America Journal 47 (1): 85. doi:10.2136/sssaj1983.03615995004700010017x.
36. Coleman, K, and DS Jenkinson. (1999). "ROTHC-26.3." A Model for the Turnover of Carbon in Soils …, no. November 1999. http://www.uni-kassel.de/~w_dec/Modellierung/wdec-rothc_manual.pdf.
37. Running, Steven W., and E. Raymond Hunt Jr. "Generalization of a forest ecosystem process model for other biomes, BIOME-BCG, and an application for global-scale models." (1993): 141.
38. Delpierre, N., E. Dufrêne, K. Soudani, E. Ulrich, S. Cecchini, J. Boé, and C. François. (2009a). "Modelling Interannual and Spatial Variability of Leaf Senescence for Three Deciduous Tree Species in France." Agricultural and Forest Meteorology 149 (6-7): 938–48. doi:10.1016/j.agrformet.2008.11.014.
39. Tilman, D. (1990). Constraints and tradeoffs: toward a predictive theory of competition and succession. Oikos, 3-15.
40. A. Praciak, et al., The CABI encyclopedia of forest trees (CABI, Oxfordshire, UK, 2013).
41. Kuzyakov, Y. (2010). Priming effects: interactions between living and dead organic matter. Soil Biology and Biochemistry, 42(9), 1363-1371.
42. Thornton, P., (2010). Biome BGC version 4.2: Theoretical Framework of Biome-BGC. Technical Documentation.
43. Liang, B., Lehmann, J., Sohi, S. P., Thies, J. E., O'Neill, B., Trujillo, L., ... & Luizão, F. J. (2010). Black carbon affects the cycling of non-black carbon in soil. Organic Geochemistry, 41(2), 206-213.
44. Walther, B. A., & Moore, J. L. (2005). The concepts of bias, precision and accuracy, and their use in testing the performance of species richness estimators, with a literature review of estimator performance. Ecography, 28(6), 815-829.
45. Keenan, T.F., Ian Baker, Alan Barr, Philippe Ciais, Ken Davis, Michael Dietze, Danillo Dragoni, et al. (2012). "Terrestrial Biosphere Model Performance for Inter-Annual Variability of Land-Atmosphere CO2 Exchange." Global Change Biology 18 (6): 1971–87. doi:10.1111/j.1365-2486.2012.02678.x.
46. Taylor, K.: Summarizing multiple aspects of model performance in a single diagram, J. Geophys. Res., 106, 7183–7192, 2001.
47. Booth, B. B. B., Jones C. D., Collins, M., Totterdell, I. J., Cox, P. M., Sitch, S., Huntingford, C., Betts, R. A., Harris, G. R., Lloyd, J. (2012), High sensitivity of future global warming to land carbon cycle processes, Environmental Research Letters 7 (2), 024002.
48. Lloyd, J., & Taylor, J. A. (1994). On the temperature dependence of soil respiration. Functional ecology, 315-323.
49. Zhao, Y., Ciais, P., Peylin, P., Viovy, N., Longdoz, B., Bonnefond, J. M., Rambal, S., Klumpp, K., Olioso, A., Cellier, P., Maignan, F., Eglin, T., and Calvet, J. C.: How errors on meteorological variables impact simulated ecosystem fluxes: a case study for six French sites, Biogeosciences, 9, 2537–2564, doi:10.5194/bg-9-2537-2012, 2012.

Preprints (www.preprints.org) | NOT PEER-REVIEWED | Posted: 17 March 2017 doi:10.20944/preprints201703.0141.v1

50. Doblas-Miranda, E., Martínez-Vilalta, J., Lloret, F., Álvarez, A., Ávila, A., Bonet, F. J., ... & Ferrandis, P. (2015). Reassessing global change research priorities in mediterranean terrestrial ecosystems: how far have we come and where do we go from here?. Global Ecology and Biogeography, 24(1), 25-43.
51. Huber-Sanwald, E., Huenneke, L. F., Jackson, R. B., Kinzig, A., Leemans, R., Lodge, D. M., ... & Walker, B. H. (2000). Biodiversityglobal biodiversity scenarios for the year 2100. Science 287: 17701774Schiffers K, Tielbrger K, Jeltsch F (2010) Changing importance of environmental factors driving secondary succession on molehills. J Veg Sci, 21, 500506Seifan.
52. T Muraoka, H., & Koizumi, H. (2005). Photosynthetic and structural characteristics of canopy and shrub trees in a cool-temperate deciduous broadleaved forest: implication to the ecosystem carbon gain. Agricultural and Forest Meteorology, 134(1), 39-59.
53. Kramer, K, I. Leinonen, H. H. Bartelink, P. Berbigier, M. Borghetti, E. Cienciala, A. J. Dolman, et al. (2002). "Evaluation of Six Process-Based Forest Growth Models Using Eddy-Covariance Measurements of CO 2 and H 2 O Fluxes at Six Forest Sites in Europe", 213–30.
54. Keenan, T., R. Garcia, S. Sabate, and C. A. Gracia. (2007). "Process Based Forest Modelling: A Thorough Validation And Future Prospects For Mediterranean Forests In A Changing World" 92: 81–92.
55. Zhou, W., Hui, D., & Shen, W. (2014). Effects of soil moisture on the temperature sensitivity of soil heterotrophic respiration: a laboratory incubation study. PloS one, 9(3), e92531.
56. Hollinger, D. Y., & Richardson, A. D. (2005). Uncertainty in eddy covariance measurements and its application to physiological models. Tree physiology, 25(7), 873-885.
57. DeLUCIA, E. V. A. N., Drake, J. E., Thomas, R. B., & GONZALEZ-MELER, M. I. Q. U. E. L. (2007). Forest carbon use efficiency: is respiration a constant fraction of gross primary production?. Global Change Biology, 13(6), 1157-1167.
58. Ito, A., & Oikawa, T. (2004). Global mapping of terrestrial primary productivity and light-use efficiency with a process-based model. Global Environmental Change in the Ocean and on Land, 343-358.
59. Sabaté, S., Gracia, C. A., & Sánchez, A. (2002). Likely effects of climate change on growth of Quercus ilex, Pinus halepensis, Pinus pinaster, Pinus sylvestris and Fagus sylvatica forests in the Mediterranean region. Forest ecology and management, 162(1), 23-37.
60. Chiti, T., Papale, D., Smith, P., Dalmonech, D., Matteucci, G., Yeluripati, J., ... & Valentini, R. (2010). Predicting changes in soil organic carbon in mediterranean and alpine forests during the Kyoto Protocol commitment periods using the CENTURY model. Soil use and management, 26(4), 475-484.
61. Dickinson, Colin Hedley. 2012. Biology of plant litter decomposition. Vol. 2. Elsevier,
62. Yang, Y., Zhu, Q., Peng, C., Wang, H., Xue, W., Lin, G., ... & Li, S. (2016). A novel approach for modelling vegetation distributions and analysing vegetation sensitivity through trait-climate relationships in China. Scientific reports, 6.
63. Yang, Y., Zhu, Q., Peng, C., Wang, H., & Chen, H. (2015). From plant functional types to plant functional traits: A new paradigm in modelling global vegetation dynamics. Progress in Physical Geography, 39(4), 514-535.
64. Messier, J., McGill, B. J., & Lechowicz, M. J. (2010). How do traits vary across ecological scales? A case for trait-based ecology. Ecology letters, 13(7), 838-848.
65. Claussen, M., L.A. Mysak, A.J. Weaver, M. Crucifix, T. Fichefet, M.-F. Loutre, S.L. Weber, J. Alcamo, V.A. Alexeev, A. Berger, R. Calov, A. Ganopolski, H. Goosse, G. Lohmann, F. Lunkeit, I.I. Mokhov, V. Petoukhov, P. Stone, and Z. Wang, 2002: Earth System Models of Intermediate Complexity: Closing the Gap in the Spectrum of Climate System Models. Climate Dyn., 18, 579-586.
66. Lavorel, S., Díaz, S., Cornelissen, J. H. C., Garnier, E., Harrison, S. P., McIntyre, S., ... & Urcelay, C. (2007). Plant functional types: are we getting any closer to the Holy Grail?. In Terrestrial ecosystems in a changing world (pp. 149-164). Springer Berlin Heidelberg.
67. Schaber, Jörg, and Franz-W Badeck. (2003). "Physiology-Based Phenology Models for Forest Tree Species in Germany." International Journal of Biometeorology 47 (4): 193–201. doi:10.1007/s00484-003-0171-5.
68. Linkosalo, T., Lappalainen, H. K., & Hari, P. (2008). A comparison of phenological models of leaf bud burst and flowering of boreal trees using independent observations. Tree Physiol, 28(12), 1873-1882.
69. Uusitalo, L., Lehikoinen, A., Helle, I., & Myrberg, K. (2015). An overview of methods to evaluate uncertainty of deterministic models in decision support. Environmental Modelling & Software, 63, 24-31.
70. Wythers, K. R., Reich, P. B., & Bradford, J. B. (2013). Incorporating temperature-sensitive Q10 and foliar respiration acclimation algorithms modifies modeled ecosystem responses to global change. Journal of Geophysical Research: Biogeosciences, 118(1), 77-90.
71. Ryan, MG, ST Gower, and RM Hubbard. (1995). "Woody Tissue Maintenance Respiration of Four Conifers in Contrasting Climates." Oecologia, 133–40.

Preprints (www.preprints.org) | NOT PEER-REVIEWED | Posted: 17 March 2017 doi:10.20944/preprints201703.0141.v1

72. Valentini, R., Matteucci, G., Dolman, A. J., Shulze, E. D., Rebmann, C. J. M. E. A. G., Moors, E. J., … $ Lindroth, A. (2000). Respiration as the main determinant of Carbon balance in European forests. Nature, 404(6780), 851-865.

© 2017 by the authors. Licensee *Preprints*, Basel, Switzerland. This article is an open access article distributed under the terms and conditions of the Creative Commons by Attribution (CC-BY) license (http://creativecommons.org/licenses/by/4.0/).